# Coordination Chemistry and QTAIM Analysis of Homoleptic Dithiocarbamate Complexes, $M(S_2CN^iPr_2)_4$, M = Ti, Zr, Hf, Th, U, Np

Andrew C. Behrle,[1] Alexander J. Myers,[1] Andrew Kerridge,[2]* and Justin R. Walensky[1]*

[1] Department of Chemistry, University of Missouri, Columbia, MO 65211-7600

[2] Department of Chemistry, Lancaster University, Lancaster LA1 4YB, UK

## Abstract

In a systematic approach to compare the molecular structure and bonding in homoleptic transition metal and actinide complexes, a series of dithiocarbamates, $M(S_2CN^iPr_2)_4$, M = Ti, Zr, Hf, Th, U, and Np have been synthesized. These complexes have been characterized through spectroscopic and X-ray crystallographic analysis, and their bonding examined using density functional theory calculations. Computational results show that covalent character associated with the metal-sulfur bonds is similar throughout the complexes studied.

## Introduction

Dithiocarbamates are an important class of ligands in the coordination chemistry of metals and main group elements. The actinides are no exception as homoleptic dithiocarbamate complexes of Th(IV),[1-2] U(IV),[3-5] Np(III),[6] Np(IV),[3,7] and Pu(IV)[3] have been reported. Due to their synthetic ease and chelating ability, dithiocarbamates have been investigated as potential candidates for separation of actinides from lanthanides,[8] an important step in the recycling of spent nuclear fuel. The use of sulfur-based ligands has shown affinity for actinides[9] over their lanthanide counterparts in previous studies.

This has brought the covalent character of actinide-ligand bonding to the forefront of research in f element chemistry[i] since the 4f orbitals are buried within the core orbitals and lack the radial extension to overlap with ligand-based orbitals. This is never a question with transition metals, which have a high degree of covalent bonding due to strong *n*d and *n*p orbital interactions.

Interestingly, density functional theory calculations in concert with X-ray Absorption Near-Edge Spectroscopy (XANES) measurements have produced a vastly different picture of bonding in the f block elements which vary with the energetics of the metal- (5f) and ligand-based (*n*p) orbitals. According to first order perturbation theory, eq 1, The mixing between actinide and ligand in a~~an actinide-ligand~~ molecular orbital is directly proportional to the overlap between metal and ligand orbitals, $\beta$, ~~and the~~with an inverse relationship between the energiesy of the ~~metal-and-ligand~~ orbitals, $\varepsilon$.[iiiii] Therefore, an actinide-ligand bond could appear more covalent than a transition metal bond due to eq 1, however, the increased ~~in~~ covalency could also be accompanied by~~also is associated with~~ a weaker metal-ligand bond. However, bond dissociation energies are rarely studied in the f elements. To continue to examine this phenomenon, our objective was to design a series of complexes with the same coordination sphere and oxidation state, hence creating a situation where the only differences are in valence orbitals, ionic radius, and the energy differences between metal and ligand-based orbitals.

**Commented [A1]:** You could mention that \beta is associated with overlap-driven covalency and \eps_f -\eps_L with degeneracy-driven covalency since this sort of language seems to be getting more popular.

$$\Psi = \Phi_f + \left[\frac{\beta}{\varepsilon_f - \varepsilon_L}\right]\Phi_L \qquad \textbf{(1)}$$

Dithiocarbamate complexes bearing isopropyl groups have been examined, but not structurally characterized, and we saw the opportunity to create a series of tetravalent complexes of group IV (Ti,[10-14] Zr,[15,16] and Hf[17]), thorium, uranium, and neptunium to investigate their molecular and electronic structures. To our surprise, no crystallographic hafnium dithiocarbamate complexes have been reported. This represents a rare study comparing transition metal and actinide elements with identical oxidation states and coordination environments, despite differences in ionic radii.[9,18]

**Experimental**

**General considerations.** The syntheses and manipulations described below were conducted using standard Schlenk and glove box techniques. All reactions were conducted in a Vacuum

Atmospheres inert atmosphere ($N_2$) glove box. $TiBr_4$, $ZrCl_4$, $HfCl_4$, $^n$BuLi, (Aldrich) were used as received. $[ThCl_4(DME)_2]$[19], $[UCl_4]$[20] and $[NpCl_4(DME)_2]$[21] were synthesized as previously described. Toluene-$d_8$ (Cambridge Isotope Laboratories), $CS_2$, and $HN^iPr_2$ (Aldrich) were dried over molecular sieves and degassed with three freeze-evacuate-thaw cycles. All $^1$H and $^{13}$C NMR data were obtained on a 300 MHz DRX Bruker spectrometer. $^1$H NMR shifts given were referenced internally to the residual solvent peak at $\delta$ 2.08 ppm ($C_7D_7H$). For paramagnetic compounds, the $^1$H NMR resonances include the peak width at half-height given in Hertz. $^{13}$C NMR shifts were referenced internally to the residual peak at $\delta$ 20.42 ppm ($C_7D_8$). Infrared spectra were recorded as KBr pellets on Perkin-Elmer Spectrum One FT-IR spectrometer. Elemental analyses were performed by Atlantic Microlab, Inc. (Norcross, GA) or University of California, Berkeley Microanalytical Facility using a Perkin Elmer Series II 2400 CHNS analyzer. Single X-ray crystal structure determinations were performed at the University of Missouri-Columbia.

**Crystallographic Data Collection and Structure Determination.** The selected single crystals for the non-neptunium complexes were mounted on nylon cryoloops using viscous hydrocarbon oil. The selected single Np crystal was coated with viscous hydrocarbon oil inside the glove box before being mounted on a nylon cryoloop using Devcon 2 Ton epoxy. X-ray data collection was performed at 173(2) or 100(2) K. The X-ray data were collected on a Bruker CCD diffractometer with monochromated Mo-K$\alpha$ radiation ($\lambda$ = 0.71073 Å). The data collection and processing utilized Bruker Apex2 suite of programs.[22] The structures were solved using direct methods and refined by full-matrix least-squares methods on F2 using Bruker SHELX-2014/7 program.[23] All non-hydrogen atoms were refined with anisotropic displacement parameters. All hydrogen atoms were placed at calculated positions and included in the refinement using a riding model. Thermal ellipsoid plots were prepared by using Olex2[24] with 50% of probability displacements for non-

hydrogen atoms. Crystal data and details for data collection for complexes **2-7** are also provided in Table 1.

**Table 1.** X-ray crystallographic data shown for complexes **2-7**.

| | **2** | **3** | **4** | **5** | **6** | **7** |
|---|---|---|---|---|---|---|
| CCDC deposit number | 1411381 | 1411382 | 1411383 | 1411384 | 1411385 | 1583533 |
| Empirical formula | $C_{28}H_{56}N_4S_8Ti$ | $C_{28}H_{56}N_4S_8Zr$ | $C_{28}H_{56}N_4S_8Hf$ | $C_{28}H_{56}N_4S_8Th$ | $C_{28}H_{56}N_4S_8U$ | $C_{28}H_{56}N_4S_8Np$ |
| Formula weight (g/mol) | 753.14 | 796.46 | 883.73 | 937.28 | 943.27 | 942.24 |
| Crystal habit, color | Prism, red | Prism, yellow | Prism, yellow | Prism, yellow | Prism, brown | Prism, red |
| Temperature (K) | 173(2) | 100(2) | 100(2) | 100(2) | 100(2) | 100(2) |
| Space group | $P2_12_12_1$ | $P2_12_12_1$ | $P2_12_12_1$ | $P2_1/c$ | $P2_1$ | $P2_1$ |
| Crystal system | Orthorhombic | Orthorhombic | Orthorhombic | Monoclinic | Monoclinic | Monoclinic |
| Volume (Å$^3$) | 3937.8(3) | 4006.4(4) | 4003.2(4) | 3996.1(6) | 2018.0(2) | 2007.8(3) |
| *a* (Å) | 13.7423(6) | 13.8180(8) | 13.8045(8) | 17.5846(15) | 10.2466(7) | 10.2184(9) |
| *b* (Å) | 14.4550(6) | 14.5805(9) | 14.5839(8) | 10.5094(9) | 14.0423(10) | 14.0444(12) |
| *c* (Å) | 19.8231(9) | 19.8855(12) | 19.8845(11) | 21.9226(19) | 14.7375(10) | 14.6986(13) |
| $\alpha$ (°) | 90.00 | 90.00 | 90.00 | 90.00 | 90.00 | 90.00 |
| $\beta$ (°) | 90.00 | 90.00 | 90.00 | 99.477(1) | 107.8860(10) | 107.8560(10) |
| $\gamma$ (°) | 90.00 | 90.00 | 90.00 | 90.00 | 90.00 | 90.00 |
| *Z* | 4 | 4 | 4 | 4 | 2 | 2 |
| Calculated density (Mg/m$^3$) | 1.270 | 1.320 | 1.466 | 1.558 | 1.552 | 1.559 |
| Absorption coefficient (mm$^{-1}$) | 0.665 | 0.715 | 3.047 | 4.173 | 4.459 | 3.027 |
| Final R indices [I > 2σ(I)] | R = 0.0215<br>$R_W$ = 0.0542 | R = 0.0190<br>$R_W$ = 0.0457 | R = 0.0121<br>$R_W$ = 0.0291 | R = 0.0218<br>$R_W$ = 0.0427 | R = 0.0298<br>$R_W$ = 0.0696 | R = 0.0199<br>$R_W$ = 0.0413 |

**Li($S_2CN^iPr_2$), 1.** An oven dried Schlenk flask was charged with $HN^iPr_2$ (1.93 g, 19.10 mmol) followed by 10 mL of THF. The reaction flask was cooled to 0 °C and $^n$BuLi (1.60 M in hexanes, 13.13 mL, 21.01 mmol) was added via syringe. The reaction was stirred for 1 hr and cooled to −78 °C. $CS_2$ (1.45g, 21.01 mmol) was added to the reaction via syringe and the reaction was allowed to stir for 0.5 hr at −78 °C. The reaction was stirred for an addition 12 hr at room temperature to yield a clean bright orange colored solution. The solvent was removed *in vacuo* to yield a tacky orange/red solid (3.45 g, 99%). $^1$H NMR ($C_7D_8$, −40 °C): $\delta$ 6.60 (sept, 1H, $^3J_{H\text{-}H}$ = 6.6 Hz, C*H*($CH_3$)$_2$), 3.76-3.72 (m, 8H, THF), 3.53 (sept, 1H, $^3J_{H\text{-}H}$ = 6.6 Hz, C*H*($CH_3$)$_2$), 1.90 (d, 6H, $^3J_{H\text{-}H}$ = 6.6 Hz, CH(C*H*$_3$)$_2$), 1.40-1.34 (m, 8H, THF), 1.02 (d, 6H, $^3J_{H\text{-}H}$ = 6.6 Hz, CH(C*H*$_3$)$_2$. $^{13}$C{$^1$H} NMR ($C_7D_8$, 25 °C): $\delta$ 211.06, 68.58 (THF), 55.43, 50.24, 25.10 (THF), 21.09, 19.57. IR (cm$^{-1}$):

2980 (s), 2922 (m), 2851 (m), 2459 (m), 1480 (s), 1420 (s), 1387 (s), 1329 (s), 1155 (s), 1146 (s), 1055 (s), 832 (m), 800 (m), 583 (m), 472 (m).

**Ti($S_2CN^iPr_2$)$_4$, 2.** An oven dried 20 mL scintillation vial was charged with **1** (300 mg, 1.64 mmol) and dissolved in toluene. The reaction mixture was cooled to −20 °C and $TiBr_4$ (147 mg, 0.399 mmol) was added to the stirring solution. An immediate color change to dark red was observed and the reaction was allowed to stir at room temperature for 12 hr. The reaction mixture was centrifuged and filtered over a bed of Celite. The reaction mixture was concentrated and layered with hexanes to yield a red microcrystalline powder (230 mg, 77%). X-ray quality crystals were grown from a THF/hexane mixture at room temperature. $^1$H NMR ($C_7D_8$, −40 °C): $\delta$ 5.27 (s, br, 4H, C*H*($CH_3$)), 3.27 (s, br, 4H, C*H*($CH_3$)), 1.51 (s, br, 24H, CH(C*H*$_3$)), 0.66 (s, br, 24H, CH(C*H*$_3$)). $^{13}$C{$^1$H} NMR ($C_7D_8$, −40 °C): $\delta$ 207.39, 51.08, 49.64, 20.58, 18.70. IR (cm$^{-1}$): 2970 (s), 2930 (m), 2872 (m), 2419 (m), 1480 (s), 1446 (s), 1384 (s), 1322 (s), 1198 (s), 1148 (s), 1043 (s), 836 (m), 800 (m), 587 (m), 477 (m). Anal. calcd. for $C_{28}H_{56}N_4S_8Ti$: C, 44.65%; H, 7.49%; N, 7.44%. Found C, 44.71%; H, 7.56%; N, 7.39%.

**Zr($S_2CN^iPr_2$)$_4$, 3.** An oven dried 20 mL scintillation via was charged with **1** (300 mg, 1.64 mmol) and dissolved in THF. The reaction mixture was cooled to −20 °C and $ZrCl_4$ (93 mg, 0.399 mmol) was added to the stirring solution. An immediate color change to orange/red was observed and the reaction was allowed to stir at room temperature for 12 hr. The reaction mixture was centrifuged and filtered over a bed of Celite. The solvent was removed and the yellow solid was extracted twice with toluene, filtered over a bed of Celite and concentrated to yield yellow microcrystalline powder (210 mg, 66%). The solvent was reduced to 1/3 its original level and layered with hexanes. X-ray quality crystals were grown from THF/hexanes mixture at room temperature. $^1$H NMR ($C_7D_8$, −40 °C): $\delta$ 5.44 (s, br, 4H, C*H*($CH_3$)), 3.20 (s, br, 4H, C*H*($CH_3$)), 1.51 (s, br, 24H,

CH(C*H*$_3$)), 0.61 (s, br, 24H, CH(C*H*$_3$)). $^{13}$C{$^1$H} NMR ($C_7D_8$, −40 °C): $\delta$ 206.31, 51.67, 49.99, 20.23, 18.60. IR (cm$^{-1}$): Anal. calcd. for $C_{28}H_{56}N_4S_8Zr$: C, 42.22%; H, 7.09%; N, 7.03%. Found C, 42.45%; H, 7.16%; N, 6.86%.

**Hf(S$_2$CN$^i$Pr$_2$)$_4$, 4.** Following the procedure for **3**, **1** (300 mg, 1.64 mmol) and $HfCl_4$ (128 mg, 0.399 mmol) yielded an orange microcrystalline precipitate (116 mg, 33%). X-ray quality crystals were grown from a THF/hexanes mixture at room temperature. $^1$H NMR ($C_7D_8$, −40 °C): $\delta$ 5.38 (s, br, 4H, C*H*(CH$_3$)), 3.18 (s, br, 4H, C*H*(CH$_3$)), 1.54 (s, br, 24H, CH(C*H*$_3$)), 0.64 (s, br, 24H, CH(C*H*$_3$)). $^{13}$C{$^1$H} NMR ($C_7D_8$, −40 °C): $\delta$ 206.25, 52.06, 49.86, 20.12, 18.31. IR (cm$^{-1}$): 2969 (s), 2928 (s), 2873 (s), 1476 (s), 1447 (s), 1373 (s), 1323 (s), 1197 (s), 1146 (s), 1042 (s), 957 (w), 856 (w), 797 (w), 582 (m), 532 (w). Anal. calcd. for $C_{28}H_{56}N_4S_8Hf$: C, 38.05%; H, 6.39%; N, 6.34%. Found C, 37.49%; H, 6.15%; N, 6.26%.

**Caution!** Thorium-232 ($t_{1/2}$ = 1.4 x10$^{10}$ years) and uranium-238 ($t_{1/2}$ = 4.5x10$^9$ years) are weak α-emitting radionuclides. This research was conducted in a radiological laboratory with appropriate counting equipment and analysis of hazards for the safe handling and manipulation of radioactive materials.

**Th(S$_2$CN$^i$Pr$_2$)$_4$, 5.** An oven dried 20 mL scintillation vial was charged with **1** (334 mg, 1.82 mmol) and dissolved in THF. $ThCl_4(DME)_2$ (246 mg, 0.444 mmol) was added to the solution at room temperature resulting in an orange/red solution and was stirred for 12 hr. The solvent was removed *in vacuo* and extracted twice with toluene, filtered over a bed of Celite and concentrated to yield a colorless precipitate (233 mg, 56%). X-ray quality crystals were grown from concentrated THF/hexane mixture at room temperature. $^1$H NMR ($C_7D_8$, −40 °C): $\delta$ 5.64 (s, br, 4H, C*H*(CH$_3$)$_2$), 3.26 (s, br, 4H, C*H*(CH$_3$)$_2$), 1.51 (s, br, 24H, CH(C*H*$_3$)$_2$), 0.68 (s, br, 24H, CH(C*H*$_3$)$_2$). $^{13}$C{$^1$H}

NMR ($C_7D_8$, −40 °C): $\delta$ 204.16, 52.81, 50.47, 20.06, 18.36. IR ($cm^{-1}$): 3003 (m), 2972 (s), 2930 (s), 2876 (m), 2414 (m), 1479 (s), 1444 (s), 1383 (s), 1319 (s), 1194 (s), 1144 (s), 1118 (m), 1039 (s), 943 (m), 835 (m), 790 (m), 584 (m), 475 (m). Anal. calcd. for $C_{28}H_{56}N_4S_8Th$: C, 35.88%; H, 6.02%; N, 5.98%. Found C, 32.45%; H, 5.30%; N, 5.07%.

**$U(S_2CN^iPr_2)_4$, 6.** An oven dried 20 mL scintillation vial was charged with **1** (349 mg, 1.90 mmol) and dissolved in THF. The reaction mixture was cooled to −20 °C and $UCl_4$ (176 mg, 0.465 mmol) was added resulting in a brown/yellow color change. The mixture was stirred for 12 hr at room temperature. The solvent was removed *in vacuo* and the solid was extracted twice with toluene, filtered over a bed of Celite, and concentrated to yield a dark brown precipitate (206 mg, 47%). X-ray quality crystals were grown from a concentrated THF/hexane mixture at room temperature. $^1H$ NMR ($C_7D_8$, −40 °C): $\delta$ 8.27 (s, br, 4H, C*H*$(CH_3)_2$, $\nu_{1/2}$ = 49 Hz), 3.76 (s, br, 4H, C*H*$(CH_3)_2$, $\nu_{1/2}$ = 49 Hz), 3.14 (s, br, 24H, CH(C*H*$_3)_2$, $\nu_{1/2}$ = 24 Hz), 1.84 (s, br, 24H, CH(C*H*$_3)_2$, $\nu_{1/2}$ = 26 Hz). IR ($cm^{-1}$): 2970 (s), 2928 (s), 2877 (m), 1474 (s), 1446 (s), 1373 (s), 1320 (s), 1192 (s), 1145 (s), 1036 (s), 933 (m), 913 (m), 849 (w), 792 (w), 584 (m), 525 (w), 473 (w). Anal. calcd. for $C_{28}H_{56}N_4S_8U$: C, 35.64%; H, 5.98%; N, 5.94%. Found C, 33.94%; H, 5.66%; N, 5.12%.

**General considerations for $^{237}$Np.**

**Caution!** $^{237}$Np is a high specific-activity α-emitting radionuclide (4.958 MeV, $t_{1/2}$ = 2.14 x$10^6$ years, $a$ = 0.7 mCi $g^{-1}$). This research was conducted in a radiological laboratory with appropriate counting equipment and analysis of hazards for the safe handling and manipulation of radioactive materials. Reactions were performed in a Vacuum Atmospheres inert atmosphere (Ar) glove box operated at negative pressure relative to the laboratory atmosphere. $^1H$ NMR spectra were recorded on a 300 MHz DRX Bruker spectrometer. Np samples were contained by placing a 4 mm PTFE

NMR tube liner inside a 5 mm glass NMR tube. Electronic absorption measurements were recorded on a sealed 1 cm quartz cuvette with a Varian Cary 5000 UV/vis/NIR spectrophotometer. **$Np(S_2CN^iPr_2)_4$, 7.** An oven dried 20 mL scintillation vial was charged with $NpCl_4(DME)_2$ (17.5 mg, 0.032 mmol) and dissolved in 1.5 mL THF. After cooling to -35 °C, the solution was added to solid **1** (23.5 mg, 0.13 mmol) resulting in red/orange color change. The mixture was stirred for 18 hr at room temperature and the solvent removed *in vacuo.* The solid was extracted twice with toluene, filtered over a bed of Celite, and the solvent removed *in vacuo* to yield a red/orange solid (20.7 mg, 70%). X-ray quality crystals were grown from a concentrated THF/hexane mixture at room temperature. $^1$H NMR ($C_7D_8$, −40 °C): $\delta$ 6.91 (s, br, 4H, C*H*$(CH_3)_2$, $\nu_{1/2}$ = 29 Hz), 2.70 (s, br, 24H, CH(C*H*$_3)_2$, $\nu_{1/2}$ = 16 Hz), 1.50 (s, br, 4H, C*H*$(CH_3)_2$, $\nu_{1/2}$ = 24 Hz), 0.41 (s, br, 24H, CH(C*H*$_3)_2$, $\nu_{1/2}$ = 13 Hz). Vis/NIR (THF, 2.0 mM, 25 °C, L·mol$^{-1}$ cm$^{-1}$): 684 (ε = 59), 746 (ε = 112), 773 (ε = 133), 789 (ε = 141), 885 (ε = 57), 891 (ε = 178), 966 (ε = 142), 952 (ε = 160), 1037 (ε = 75), 1578 (ε = 39), 1867 (ε = 30).

**Computational Details**

All calculations were performed at the density functional theoretical (DFT) level using version 6.6 of the TURBOMOLE quantum chemistry software package.[25] XRD-derived structural parameters were used as the basis for geometry optimizations. The hybrid-GGA PBE0[26] exchange-correlation functional, which incorporates a perturbatively derived 25% contribution of exact exchange, was used throughout. In all calculations, basis sets of polarized triple-ζ quality were used. For geometry optimizations, Ahlrichs-style basis sets[27,28] were employed, incorporating effective core potentials replacing 28 core electrons of Zr and 60 core electrons of Hf, Th, U and Np.[29-30] We have successfully applied this model chemistry in previous studies of f-element complexes.[31-33] All

complexes considered in this study were identified as energetic minima through vibrational frequency analysis.

Topological properties of the resulting electron densities were obtained via application of the Quantum Theory of Atoms in Molecules[34] (QTAIM) as implemented in version 14.11.23 of the AIMAll code.[35] In order to perform analysis of integrated properties of the density via QTAIM, all-electron single point energy calculations were performed at the optimized geometries. These calculations employed the Zr TZVPalls2 basis set of Ahlrichs and May[36] and the Hf, Th, U and Np SARC basis sets of Pantazis and Neese[37,38] and incorporated scalar relativistic effects via the 2nd order Douglas-Kroll-Hess Hamiltonian.

**Results**

The isopropyl derivative was targeted for its solubility properties in arene solvents which made for facile isolation. Deprotonation of $HN^iPr_2$ with $^n$BuLi followed by addition of $CS_2$ affords $LiS_2CN^iPr_2$, **1**. Reaction of four equivalents of **1** with $MCl_4$ yields the corresponding homoleptic metal dithiocarbamate complexes, $M(S_2CN^iPr_2)_4$, M = Ti, **2**; Zr, **3**; Hf, **4**; Th, **5**; U, **6**, Np, **7**, eq 2, in moderate to good crystalline yields.

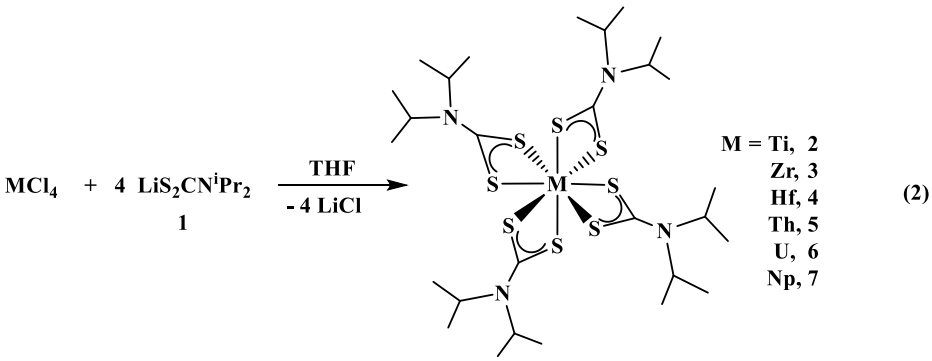


(2)

All complexes displayed fluxional behavior in solution as observed using $^{1}$H NMR spectroscopy at room temperature. This has been seen previously[39] with this ligand set hence $^{1}$H NMR spectra were taken at -40 °C. Resonances for the isopropyl methyl and methine protons are summarized in Table 2. The resonances do not show any particular pattern for the diamagnetic species, but are paramagnetically shifted for the uranium(IV) and neptunium(IV) complexes. The visible and near-infrared spectrum (Supporting Information) of **7** showed similar features to those observed in $Np[S_2P(C_6H_5)_2]_4$.[40]

**Table 2.** $^{1}$H NMR resonances for the isopropyl methyl and methine protons for complexes **1**-**7**.

| Complex, M | $CH(CH_3)_2$ $^{1}$H NMR resonances (ppm) | $CH(CH_3)_2$ $^{1}$H NMR resonances (ppm) |
|---|---|---|
| **1, Li** | 1.90, 1.02 | 6.60, 3.53 |
| **2, Ti** | 1.51, 0.66 | 5.27, 3.27 |
| **3, Zr** | 1.51, 0.61 | 5.44, 3.20 |
| **4, Hf** | 1.54, 0.64 | 5.38, 3.18 |
| **5, Th** | 1.51, 0.68 | 5.64, 3.26 |
| **6, U** | 3.14, 1.84 | 8.27, 3.76 |
| **7, Np** | 2.70, 0.41 | 6.91, 1.50 |

The solid-state structures of complexes **2**-**7** were determined using X-ray crystallography analysis with selected bond distances shown in Table 3. Representative examples, complexes **4** and **7**, are shown in Figure 1. Each complex is eight-coordinate in a trigonal dodecahedron arrangement about the metal center. The metal-sulfur bond distances mimic the ionic radii of these complexes with the shortest metal-sulfur distances found with titanium ($r$ = 0.74 Å) and the longest with thorium ($r$ = 1.05 Å).[41] The metal-sulfur bond lengths are similar to others reported. For example,

the average Ti-S bond distance of 2.552 Å in **1** is similar to the range of bond lengths of 2.522(8) – 2.606(8) Å in $Ti(S_2CNEt_2)_4$.[10] In **2**, an average Zr-S bond distance of 2.655 Å was observed, which is similar to 2.69 Å in $(C_5H_5)Zr(S_2CNMe_2)_3$.[42] While no dithiocarbamate ligated complexes of hafnium could be found, the average Hf-S bond distance of 2.640 Å in **4** is significantly longer than the Hf-thiolate distances of 2.502(1) Å in $(C_5Me_5)_2Hf(SPh)_2$.[43] The homoleptic complexes, $An(S_2CNEt_2)_4$, An = Th,[2] Np,[7] compare well with the average Th-S and Np-S distances of 2.87 Å (2.870 in **5**) and 2.795 Å (2.787 Å in **7**). The average U-S bond length of 2.803 Å in **6** is similar to the U-S distances of 2.801(7) and 2.810(7) Å in $[(C_8H_8)U(S_2CNEt_2)(THF)_2][BPh_4]$.[5]

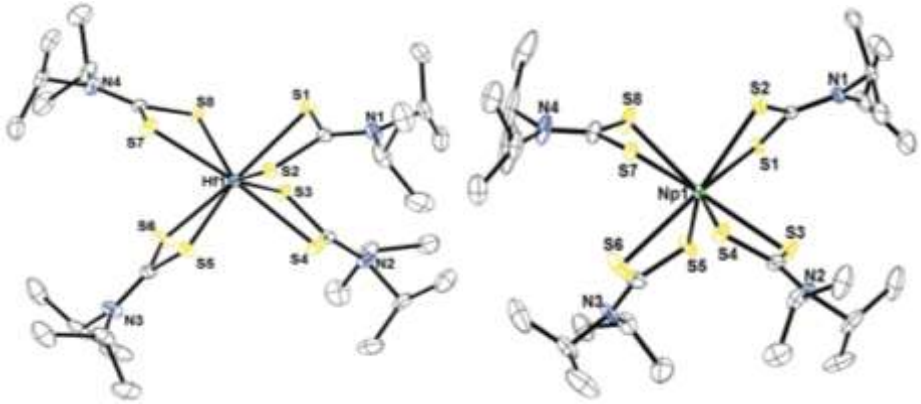


**Figure 1.** Thermal ellipsoid plots of **4** (left) and **7** (right) shown at the 50% probability level. The hydrogen atoms have been omitted for clarity.

**Table 3.** Selected bond distances (Å) and angles (deg) for complexes **2-7**.

| | **2, Ti** | **3, Zr** | **4, Hf** | **5, Th** | **6, U** | **7, Np** |
|---|---|---|---|---|---|---|
| M1-S1 | 2.5154(4) | 2.6471(6) | 2.6185(6) | 2.8824(8) | 2.818(3) | 2.7640(8) |

| | | | | | | |
|---|---|---|---|---|---|---|
| M1-S2 | 2.6086(4) | 2.6509(6) | 2.6728(6) | 2.8445(7) | 2.791(3) | 2.7791(11) |
| M1-S3 | 2.5873(4) | 2.6635(6) | 2.6500(6) | 2.9016(7) | 2.835(2) | 2.7878(11) |
| M1-S4 | 2.5200(4) | 2.6488(6) | 2.6279(6) | 2.8557(8) | 2.788(3) | 2.7928(7) |
| M1-S5 | 2.5727(4) | 2.6614(6) | 2.6528(6) | 2.8731(7) | 2.800(3) | 2.8079(9) |
| M1-S6 | 2.5288(5) | 2.6487(6) | 2.6299(6) | 2.8811(8) | 2.8078(19) | 2.7786(9) |
| M1-S7 | 2.5598(4) | 2.6827(6) | 2.6382(6) | 2.8530(7) | 2.806(3) | 2.7762(9) |
| M1-S8 | 2.5253(4) | 2.6371(6) | 2.6303(6) | 2.8725(8) | 2.781(2) | 2.7992(10) |
| S1-M1-S2 | 66.872(14) | 65.581(18) | 65.635(19) | 61.68(2) | 62.74(6) | 63.31(3) |
| S1-M1-S6 | 156.435(16) | 160.746(19) | 158.45(2) | 167.57(2) | 162.92(8) | 161.31(3) |

**Computational Results**

**Structural parameters.** The M-S bond lengths, averaged over the 8 bonds in each complex, are compared in Table 4. Theoretical values are in very good agreement with experiment, typically accurate to within 0.01 Å.

**Table 4**. Comparison of experimental and theoretical M-S bond lengths in $M(S_2CN^iPr_2)_4$ (M = Ti, Zr, Hf, Th, U, Np). Mean average deviations are given in parentheses. All values are in Å.

| Complex | Exp | PBE0 |
|---|---|---|
| $Ti(S_2CN^iPr_2)_4$ | 2.552 (0.001) | 2.548 (0.048) |
| $Zr(S_2CN^iPr_2)_4$ | 2.655 (0.002) | 2.665 (0.019) |
| $Hf(S_2CN^iPr_2)_4$ | 2.640 (0.002) | 2.665 (0.022) |
| $Th(S_2CN^iPr_2)_4$ | 2.870 (0.002) | 2.879 (0.001) |
| $U(S_2CN^iPr_2)_4$ | 2.803 (0.008) | 2.809 (0.012) |
| $Np(S_2CN^iPr_2)_4$ | 2.787 (0.003) | 2.799 (0.008) |

**Topological properties of the electron density**

Properties of the electron density at QTAIM derived M-S bond critical points (BCPs) are summarized in Table 5. While these properties are indicative of predominantly ionic interactions,

the magnitude of the electron density at the M-S BCP of the U and Np complexes are noticeably higher than in the thorium analogue, implying greater covalency in the former two. This trend is mirrored by the BCP energy densities *H*, and are as seen previously,[33,44] although the difference between values obtained for uranium/neptunium and thorium complexes is less pronounced here. When considering the transition metal complexes, no periodic trend is found, although the degree of covalency is very similar in all complexes, and comparable to that found in the uranium/neptunium analogues.

**Table 5**. Topological properties at the M-S bond critical points (BCPs) of the PBE0-derived electron densities. $\rho$ = electron density, $\nabla^2\rho$ = Laplacian of the density, *H* = energy density. All values are in a.u.

| Complex | $\rho$ | $\nabla^2\rho$ | *H* |
|---|---|---|---|
| $Ti(S_2CN^iPr_2)_4$ | 0.055 (4×0.050, 4×0.060) | 0.089 | -0.0113 |
| $Zr(S_2CN^iPr_2)_4$ | 0.055 (4×0.053,4×0.057) | 0.082 | -0.0126 |
| $Hf(S_2CN^iPr_2)_4$ | 0.054 (4×0.052,4×0.057) | 0.081 | -0.0134 |
| $Th(S_2CN^iPr_2)_4$ | 0.052 | 0.063 | -0.0117 |
| $U(S_2CN^iPr_2)_4$ | 0.056 | 0.078 | -0.0134 |
| $Np(S_2CN^iPr_2)_4$ | 0.056 | 0.078 | -0.0135 |

**Integrated properties of the electron density**

The QTAIM definition of an atom allows for the evaluation of both one- and two-electron integrated properties. The atomic charge *q* (a one-electron property) and the localization and delocalization indices $\lambda$ and $\delta$ (two-electron properties) are summarized for Ti, Zr, Hf, Th, U, Np, and S in Table 6. Here, a periodic trend is found: the atomic charge increases from Ti to Hf, while the sulfur charge drops, suggesting increased ionic interaction. Consideration of the two-electron properties support this assertion: the M-S delocalization indices (the number of electrons shared between the two atoms), which can be considered an alternative measure of covalent character,[33,44-47] decrease from Ti to Hf, implying a reduction in covalent character. The one- and two-electron

data combined therefore describe a weak transition in the nature of the M-S bond from Ti to Hf. The data supports the characterization of neptunium as exhibiting greater covalent character then thorium or uranium and, in fact, imply that the Np-S bond is the most covalent of any considered here. Our previous work on dithiophosphinate and diselenophosphinate actinide complexes[33,44] led us to conclude that delocalization indices provided a more robust description of covalency than that provided by topological properties of the electron density alone. The delocalization indices for the thorium and uranium complexes are very similar to those observed in dithiophosphinate and dithiophosphonate complexes.[33,44]

We have previously noted that the difference between atomic number *Z* and localization index $\lambda$ correlates with oxidation state in f-element complexes[33,45,46] and we also find this correlation here: Z - $\lambda$ values fall in the range 3.79 - 4.33, close to the formal +4 oxidation state and with a trend towards larger values for heavier elements.

**Table 6**. Integrated QTAIM properties of the PBE0-derived electron densities. $q$ = atomic charge, $\lambda$ = localization index, $\delta$ = delocalization index. All values are in a.u.

| Complex | $q$(M) | $\lambda$(M) | $q$(S) | $\delta$(M, S) |
|---|---|---|---|---|
| $Ti(S_2CN^iPr_2)_4$ | +1.89 | 18.21 | -0.14 | 0.438 |
| $Zr(S_2CN^iPr_2)_4$ | +2.15 | 36.05 | -0.19 | 0.416 |
| $Hf(S_2CN^iPr_2)_4$ | +2.28 | 68.00 | -0.21 | 0.400 |
| $Th(S_2CN^iPr_2)_4$ | +2.43 | 85.74 | -0.25 | 0.421 |
| $U(S_2CN^iPr_2)_4$ | +2.23 | 87.67 | -0.22 | 0.481 |
| $Np(S_2CN^iPr_2)_4$ | +2.17 | 88.73 | -0.21 | 0.482 |

**Discussion**

Few studies have been conducted comparing the molecular and electronic structure of transition metal and actinide complexes. In one report, the bonding in $(C_5Me_5)_2MCl_2$, M = Ti, Zr, Hf, Th, and U complexes were compared and concluded that half the amount of covalent character was observed in the uranium-chloride bond versus the transition metal analogs.[18] In that study, titanium had the greatest covalent character. Interestingly, when looking at $MCl_6^{2-}$ complexes, the

same group concluded that $UCl_6^{2-}$ had a greater covalent character in the metal-chloride bond than the transition metal analogs.[9] In this study, we have also examined homoleptic transition metal and actinide complexes and, while admittedly, only based on QTAIM calculations, an increase in covalent character between actinide-sulfur bonds is observed in comparison to their transition metal counterparts. The similarity between $MCl_6^{2-}$ and $M(S_2CN^iPr_2)_4$ is related in their homoleptic nature as well as the energy levels of the 3p orbitals versus the 5f orbitals of the actinides.

**Conclusion**

The elucidation of the role of the valence orbitals of the actinides remains a challenge. Here, we investigated the homoleptic dithiocarbamate complexes, $M(S_2CN^iPr_2)_4$, M = Ti, Zr, Hf, Th, U, and Np, and have shown using density functional theory that these complexes show higher degree of covalent bonding in the actinide complexes than the Group IV analogs. Interestingly, this ordering does not match previous studies with $(C_5Me_5)_2MCl_2$, M = Ti, Zr, Hf, Th, U; however, the homoleptic system, $MCl_6^{2-}$, M = Ti, Zr, Hf, U, has a similar ordering to the complexes reported here. We submit these findings, along with the previous studies identified, as an interesting phenomenon to the actinide community to discuss, for which far more work is needed to reach a satisfactory conclusion.

**Acknowledgements**

This material is based upon work supported by the U.S. Department of Homeland Security under Grant Award Number, 2012-DN-130-NF0001-02 (Ti, Zr, Hf, Th, and U). The views and conclusions contained in this document are those of the authors and should not be interpreted as necessarily representing the official policies, either expressed or implied, of the U.S. Department of Homeland Security. We thank Dr. Andrew J. Gaunt for guidance in the synthesis of

$NpCl_4(DME)_2$. J.R.W. gratefully acknowledges support for the Np work from the U.S. Department of Energy, Office of Science, Early Career Research Program under Award Number DE-SC-0014174. A.K. thanks the EPSRC for the award of a Career Acceleration Fellowship (grant award number EP/J002208/2) and Lancaster University for access to the HEC HPC facility.

**References**

(1) Bagnall, K. W.; Yanir, E., Thorium(IV) and uranium(IV) carbamates. *J. Inorg. Nucl. Chem.* **1974**, *36*, 777-779.

(2) Brown, D.; Holah, D. G.; Rickard, C. E. F., Structure of thorium(IV) tetrakis-(NN-diethyldithiocarbamate). *J. Chem. Soc. A.* **1970**, 423-425.

(3) Bagnall, K. W.; Brown, D.; Holah, D. G., Actinide(IV)N,N-diethyldithiocarbamate complexes. *J. Chem. Soc. A.* **1968**, 1149-1153.

(4) Bibler, J. P.; Karraker, D. G., Diethyldithiocarbamates of quadrivalent actinides. *Inorg. Chem.* **1968**, *7*, 982-985.

(5) Boisson, C.; Berthet, J. C.; Ephritikhine, M.; Lance, M.; Nierlich, M., Reactivity of the cationic uranium amide compound $[U(\nu\text{-}C_8H_8)(NEt_2(OC_4H_8)_2][BPh_4]$. *J. Organomet. Chem.* **1996**, *522*, 249-257.

(6) Brown, D.; Holah, D. G.; Rickard, C. E. F., NN-diethyldithiocarbamate complexes of trivalent lanthanide and actinide elements and the crystal structure of tetraethylammonium neptunium(III) tetrakis-(NN-diethyldithiocarbamate). *J. Chem. Soc. A.* **1970**, 786-790.

(7) Charushnikova, I. A.; Fedoseev, A. M.; Polyakova, I. N., Crystal structure of neptunium(IV) N,N-diethyl dithiocarbamate $Np[S_2CN(C_2H_5)_2]_4$. *Russ. J. Coord. Chem.* **2006,** *32*, 751-755.

(8) Miyashita, S.; Satoh, I.; Yanaga, M.; Okuno, K.; Suganuma, H., Separation of Am(III) from Eu(III) by extraction based on in situ extractant formation of dithiocarbamate derivatives. *Prog. Nucl. Energ.* **2008**, *50*, 499-503.

(9) Minasian, S. G.; Keith, J. M.; Batista, E. R.; Boland, K. S.; Clark, D. L.; Conradson, S. D.; Kozimor, S. A.; Martin, R. L.; Schwarz, D. E.; Shuh, D. K.; Wagner, G. L.; Wilkerson, M. P.; Wolfsberg, L. E.; Yang, P., Determining Relative f and d Orbital Contributions to M–Cl Covalency in $MCl_6^{2-}$ (M = Ti, Zr, Hf, U) and $UOCl^{5-}$ Using Cl K-Edge X-ray Absorption Spectroscopy and Time-Dependent Density Functional Theory. *J. Am. Chem. Soc.* **2012**, *134*, 5586-5597.

(10) Colapietro, M.; Vaciago, A.; Bradley, D. C.; Hursthouse, M. B.; Rendall, I. F., Structural studies of metal dithiocarbamates. Part VI. The crystal and molecular structure of tetrakis(NN-diethyldithiocarbamato)titanium(IV). *J. Chem. Soc., Dalton Trans.* **1972**, 1052-1057.

(11) Bhat, A. N.; Fay, R. C.; Lewis, D. F.; Lindmark, A. F.; Strauss, S. H., Preparation and characterization of some six-, seven-, and eight-coordinate titanium(IV) N, N-dialkyldithiocarbamates. *Inorg. Chem.* **1974**, *13*, 886-892.

(12) Bradley, D. C.; Gitlitz, M. H., Preparation and properties of NN-dialkyldithiocarbamates of early transition elements. *J. Chem. Soc. A.* **1969**, 1152-1156.

(13) Colapietro, M.; Vaciago, A.; Bradley, D. C.; Hursthouse, M. B.; Rendall, I. F., The crystal structure of tetrakis-(NN-diethyldithiocarbamato)titanium(IV), an eight-co-ordinated titanium compound. *J. Chem. Soc., Chem. Commun.* **1970**, 743-744.

(14) Bradley, D. C.; Gitlitz, M. H., NN-Dialkyldithiocarbamates of transition-metals of Groups IV and V. *Chem. Commun.* **1965**, 289.

(15) Bradley, D. C.; Rendall, I. F.; Sales, K. D., Covalent compounds of quadrivalent transition metals. Part VI. Spectroscopic studies on titanium, vanadium, and zirconium diethyldithiocarbamates. *J. Chem. Soc., Dalton Trans.* **1973**, 2228-2233.

(16) Lindmark, A. F.; Fay, R. C., Kinetics of hindered rotation about carbon-nitrogen single bonds in some N,N-diisopropyldithiocarbamates. *Inorg. Chem.* **1983**, *22*, 2000-2006.

(17) Behnam-Dehkordy, M.; Crociani, B.; Nicolini, M.; Richards, R. L., The reactions of t-BuNC with halides of Titanium(IV), Hafnium(IV), Vanadium(III), Niobium(IV), Molybdenum(V) and Tungsten(VI); insertion into metal—halogen bonds and ligand displacement reactions. *J. Organomet. Chem.* **1979**, *181*, 69-80.

(18) Kozimor, S. A.; Yang, P.; Batista, E. R.; Boland, K. S.; Burns, C. J.; Clark, D. L.; Conradson, S. D.; Martin, R. L.; Wilkerson, M. P.; Wolfsberg, L. E., Trends in Covalency for d- and f-Element Metallocene Dichlorides Identified Using Chlorine K-Edge X-ray Absorption Spectroscopy and Time-Dependent Density Functional Theory. *J. Am. Chem. Soc.* **2009**, *131*, 12125-12136.

(19) Cantat, T.; Scott, B. L.; Kiplinger, J. L., Convenient access to the anhydrous thorium tetrachloride complexes $ThCl_4(DME)_2$, $ThCl_4(1,4\text{-dioxane})_2$ and $ThCl_4(THF)_{3.5}$ using commercially available and inexpensive starting materials. *Chem. Commun.* **2010**, *4*, 919-921.

(20) Gray, D. L.; Backus, L. A.; Krug von Nidda, H.-A.; Skanthakumar, S.; Loidl, A.; Soderholm, L.; Ibers, J. A., A U(V) Chalcogenide: Synthesis, Structure, and Characterization of $K_2Cu_3US_5$. *Inorg. Chem.* **2007,** *46*, 6992-6996.

(21) Reilly, S. D.; Brown, J. L.; Scott, B. L.; Gaunt, A. J., Synthesis and characterization of $NpCl_4(DME)_2$ and $PuCl_4(DME)_2$ neutral transuranic An(iv) starting materials. *Dalton Trans.* **2014,** *43*, 1498-1501.

(22) *APEX2 Suite*, Madison, WI, **2006**.

(23) Sheldrick, G., Crystal structure refinement with SHELXL. *Acta Crystallogr. C.* **2015**, *71*, 3-8.

(24) Dolomanov, O. V.; Bourhis, L. J.; Gildea, R. J.; Howard, J. A. K.; Puschmann, H., OLEX2: a complete structure solution, refinement and analysis program. *J. Appl. Cyst.* **2009**, *42*, 339-341.

(25) Ahlrichs, R.; Bär, M.; Häser, M.; Horn, H.; Kölmel, C., Electronic structure calculations on workstation computers: The program system turbomole. *Chem. Phys, Lett.* **1989**, *162*, 165-169.

(26) Adamo, C.; Barone, V., Toward reliable density functional methods without adjustable parameters: The PBE0 model. *J. Chem. Phys.* **1999**, *110*, 6158-6170.

(27) Weigend, F.; Ahlrichs, R., Balanced basis sets of split valence, triple zeta valence and quadruple zeta valence quality for H to Rn: Design and assessment of accuracy. *Phys. Chem. Chem. Phys.* **2005**, *7*, 3297-3305.

(28) Cao, X.; Dolg, M., Segmented contraction scheme for small-core actinide pseudopotential basis sets. *Journal of Molecular Structure: THEOCHEM* **2004**, *673*, 203-209.

(29) Andrae, D.; Häußermann, U.; Dolg, M.; Stoll, H.; Preuß, H., Energy-adjustedab initio pseudopotentials for the second and third row transition elements. *Theor. Chim. Acta* **1990**, *77*, 123-141.

(30) Küchle, W.; Dolg, M.; Stoll, H.; Preuss, H., Energy-adjusted pseudopotentials for the actinides. Parameter sets and test calculations for thorium and thorium monoxide. *J. Chem. Phys.* **1994**, *100*, 7535-7542.

(31) Hashem, E.; Swinburne, A. N.; Schulzke, C.; Evans, R. C.; Platts, J. A.; Kerridge, A.; Natrajan, L. S.; Baker, R. J., Emission spectroscopy of uranium(iv) compounds: a combined synthetic, spectroscopic and computational study. *RSC Adv.* **2013**, *3*, 4350-4361.

(32) Woodall, S. D.; Swinburne, A. N.; lal Banik, N.; Kerridge, A.; Di Pietro, P.; Adam, C.; Kaden, P.; Natrajan, L. S., Neptunyl(vi) centred visible LMCT emission directly observable in the presence of uranyl(vi). *Chem. Commun.* **2015**, *51*, 5402-5405.

(33) Behrle, A. C.; Kerridge, A.; Walensky, J. R., Dithio- and Diselenophosphinate Thorium(IV) and Uranium(IV) Complexes: Molecular and Electronic Structures, Spectroscopy, and Transmetalation Reactivity. *Inorg. Chem.* **2015**, *54*, 11625-11636.

(34) R. F. W. Bader, Atoms in Molecules: A Quantum Theory, Oxford University Press, Oxford, **1990**.

(35) T. A. Keith, AIMA11 (Version 14.11.23), TK Gristmill Software, Overl. Park KS, USA, **2014**.

(36) Ahlrichs, R.; May, K., Contracted all-electron Gaussian basis sets for atoms Rb to Xe. *Phys. Chem. Chem. Phys.* **2000**, *2*, 943-945.

(37) Pantazis, D. A.; Chen, X.-Y.; Landis, C. R.; Neese, F., All-Electron Scalar Relativistic Basis Sets for Third-Row Transition Metal Atoms. *J. Chem. Theory Comput.* **2008**, *4*, 908-919.

(38) Pantazis, D. A.; Neese, F., All-Electron Scalar Relativistic Basis Sets for the Actinides. *J. Chem. Theory Comput.* **2011**, *7*, 677-684.

(39) Muetterties, E. L., Solution state, nuclear magnetic resonance spectral features for tetrakis(N-methyl-N-(perfluorophenyl)dithiocarbamato)zirconium(IV). *Inorg. Chem.* **1974**, *13*, 1011-1012.

(40) Macor, J. A.; Brown, J. L.; Cross, J. N.; Daly, S. R.; Gaunt, A. J.; Girolami, G. S.; Janicke, M. T.; Kozimor, S. A.; Neu, M. P.; Olson, A. C.; Reilly, S. D.; Scott, B. L., Coordination chemistry of 2,2'-biphenylenedithiophosphinate and diphenyldithiophosphinate with U, Np, and Pu. *Dalton Trans.* **2015,** *44*, 18923-18936.

(41) Shannon, R., Revised effective ionic radii and systematic studies of interatomic distances in halides and chalcogenides. *Acta Crystallogr. A.* **1976**, *32*, 751-767.

(42) Bruder, A. H.; Fay, R. C.; Lewis, D. F.; Sayler, A. A., Synthesis, characterization, and x-ray structure of $\eta^5$-cyclopentadienyltris(N,N-dimethyldithiocarbamato)zirconium(IV). *J. Am. Chem. Soc.* **1976**, *98*, 6932-6938.

(43) Yam, V. W.-W.; Qi, G.-Z.; Cheung, K.-K., Synthesis, Emission, and Molecular Orbital Studies of Luminescent Hafnium Thiolate Complexes. Crystal Structures of $(\eta^5\text{-}C_5Me_5)_2Hf(SR)_2$ (R = $^n$Bu, $C_6H_5$, $C_6H_4$OMe-p). *Organometallics* **1998**, *17*, 5448-5453.

(44) Behrle, A. C.; Barnes, C. L.; Kaltsoyannis, N.; Walensky, J. R., Systematic Investigation of Thorium(IV)– and Uranium(IV)–Ligand Bonding in Dithiophosphonate, Thioselenophosphinate, and Diselenophosphonate Complexes. *Inorg. Chem.* **2013**, *52*, 10623-10631.

(45) Kerridge, A., Oxidation state and covalency in f-element metallocenes (M = Ce, Th, Pu): a combined CASSCF and topological study. *Dalton Trans.* **2013**, *42*, 16428-16436.

(46) Kerridge, A., f-Orbital covalency in the actinocenes (An = Th-Cm): multiconfigurational studies and topological analysis. *RSC Adv.* **2014,** *4*, 12078-12086.

(47) Kerridge, A., Quantification of f-element covalency through analysis of the electron density: insights from simulation. *Chem. Commun.* **2017,** *53*, 6685-6695.

[i] Nat. Commun. 2017, 8, 16053
[ii] Inorg. Chem. 2010, 49, 10007
[iii] J. Am. Chem. Soc. 2013, 135, 10742